ADVANCED MATERIALS

www.advmat.de

Mushrooms as Efficient Solar Steam-Generation Devices

*Ning Xu, Xiaozhen Hu, Weichao Xu, Xiuqiang Li, Lin Zhou, Shining Zhu, and Jia Zhu**

Solar steam generation is emerging as a promising technology, for its potential in harvesting solar energy for various applications such as desalination and sterilization. Recent studies have reported a variety of artificial structures that are designed and fabricated to improve energy conversion efficiencies by enhancing solar absorption, heat localization, water supply, and vapor transportation. Mushrooms, as a kind of living organism, are surprisingly found to be efficient solar steam-generation devices for the first time. Natural and carbonized mushrooms can achieve ≈62% and ≈78% conversion efficiencies under 1 sun illumination, respectively. It is found that this capability of high solar steam generation is attributed to the unique natural structure of mushroom, umbrella-shaped black pileus, porous context, and fibrous stipe with a small cross section. These features not only provide efficient light absorption, water supply, and vapor escape, but also suppress three components of heat losses at the same time. These findings not only reveal the hidden talent of mushrooms as low-cost materials for solar steam generation, but also provide inspiration for the future development of high-performance solar thermal conversion devices.

Solar steam generation has received tremendous attention for its potential in harvesting solar energy for various applications such as desalination and sterilization. Over the past few years, a variety of artificial structures have been designed and fabricated to improve energy conversion efficiency by enhancing solar absorption,[1–13] heat localization,[1,3–6,14–18] water supply, and vapor transportation.[9,15,16,18–21] Here, through careful study, for the first time, we have found that one kind of living organism, mushrooms, can enable efficient solar steam generation due to their unique structures. Under 1 sun illumination, solar steam-generation efficiencies can achieve ≈62% and ≈78%, for natural and carbonized mushrooms, respectively.

We found that this capability of high-efficiency solar steam generation was attributed to the unique natural structures of mushrooms, including their umbrella-shaped black pileus, porous context, and fibrous stipe with a small cross section. These features enabled efficient absorption of sunlight and suppressed three components of heat loss. These findings provide inspiration for the future development of high-performance devices for solar thermal conversion.

N. Xu, Dr. X. Hu, W. Xu, X. Li, Prof. L. Zhou, Prof. S. Zhu, Prof. J. Zhu
National Laboratory of Solid State Microstructures
College of Engineering and Applied Sciences and Collaborative Innovation Centre of Advanced Microstructures
Nanjing University
Nanjing 210093, China
E-mail: jiazhu@nju.edu.cn

DOI: 10.1002/adma.201606762

Mushrooms, which are widely collected for food,[21–30] seem to be surprising candidates for efficient solar steam generation (**Figure 1**a), as these fruiting bodies of fungus do not have the ability to photosynthesize[29] and typically live in an environment without much exposure to solar illumination. Thanks to the tremendous progress in the past few years, it has become clear that there are several necessary elements to enable high-performance solar steam generation, which include efficient and broadband light absorption and effective heat management without compromising water supply and vapor escape.[13,15,16,18,19] A typical mushroom (e.g., the shiitake mushroom), with a natural structure comprising an umbrella-shaped black pileus, porous context, and a fibrous stipe with a small cross section (Figure 1b), does possess all these elements. First, the umbrella-shaped black pileus can enable efficient solar absorption. This absorption can be further improved with a convenient carbonization treatment. The hydrophilic fibrous stipe can provide a sufficient water supply, which is pumped into the mushroom by capillary force. The porous context not only acts as a bridge to pump the water further into the top pileus but also provides sufficient vapor channels. The geometry of mushrooms is also naturally optimized for minimizing all three components of heat loss, which include conduction, convection, and radiation. The ratio of the diameters of black pilei and fibrous stipes is typically ≈6:1, which provides mushrooms with an effective thermal concentration structure for suppressing heat conduction loss to bulk water.[14,15] In addition, the umbrella-shaped pileus with a large surface-to-projected area ratio of ≈1.8:1 not only provides a large surface area for evaporation but also minimizes the loss from radiation and convection. All of these features are carefully elucidated below.

Figure 1b,c shows typical pictures of an umbrella-shaped shiitake mushroom before and after carbonization (details in the Experimental Section). It is obvious that the entire structure of the mushroom shrinks by ≈30% after carbonization. The structures of three components, the pileus, context, and stipe, before (Figure 1d–f) and after carbonization (Figure 1g–i) were carefully examined by scanning electron microscopy (SEM). Figure 1e presents the porous structures of a context, which has an average pore size of ≈7.5 μm (Figure S1a, Supporting Information); these pores serve as channels for efficient vapor escape. The context is in direct connection with the stipe, which is composed of coarse fibers parallel aligned along the

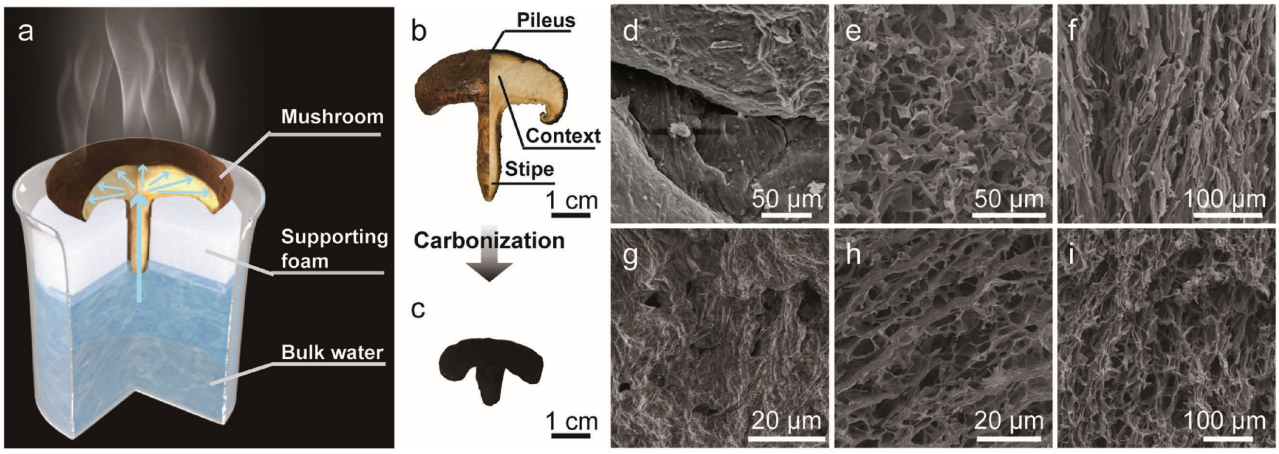

Figure 1. Mushroom-based solar steam generation. a) Schematic of a mushroom-based solar steam-generation device. b) Physical picture of a shiitake mushroom. c) Physical picture of a mushroom after carbonization. d–f) SEM images of the pileus, context, and stipe of a mushroom, respectively. g–i) SEM images of the pileus, context, and stipe of a mushroom after carbonization, respectively.

axial direction (Figure 1f). The porous and fibrous structures provide channels ideal for supplying water. After carbonization, the surface roughness of the pileus increases (Figure 1g), which is beneficial for light absorption,[31–35] as described later. The average pore size of the context decreases to 3.6 μm (Figure S1b, Supporting Information), and the microfibers in the stipe also shrink in diameter by ≈50% (Figure 1i). The carbonized mushroom maintains a porosity similar to that of the natural one, ≈90% (Table S1, Supporting Information).

The absorption of a shiitake mushroom before and after carbonization was carefully measured with an ultraviolet–visible–near-infrared spectrophotometer equipped with an integrating sphere. As shown in **Figure 2**a, a natural shiitake mushroom had an ≈79% absorption of solar energy (weighted under

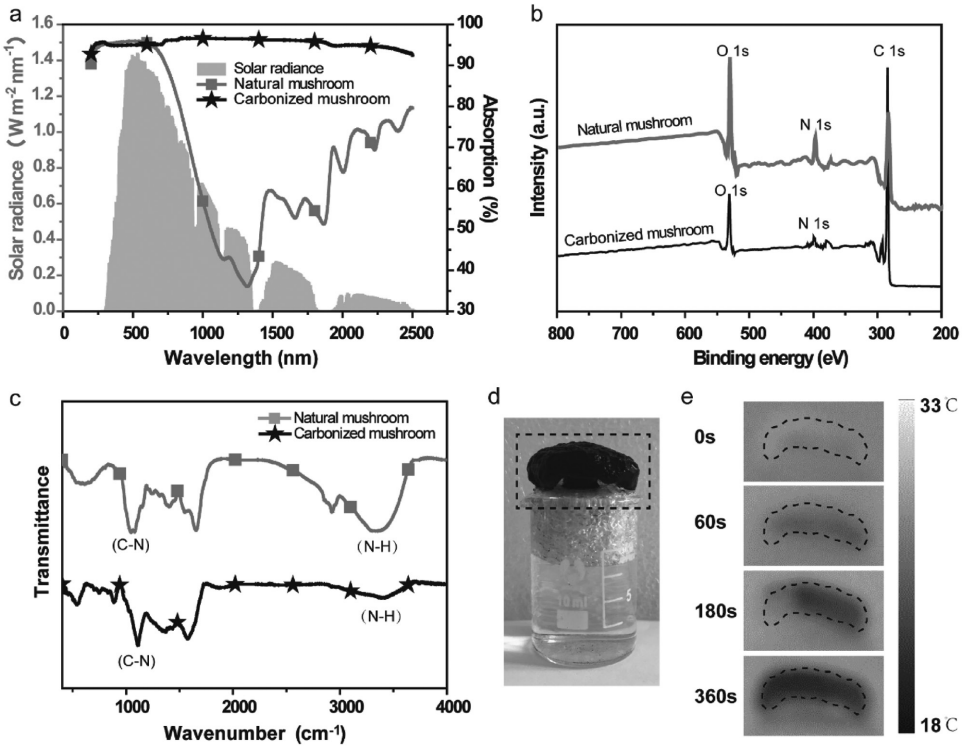

Figure 2. Absorption and hydrophilicity of natural and carbonized mushrooms. a) Solar spectral irradiance (AM 1.5 G) (gray, left hand side axis) and absorption (black, right hand side axis) of natural and carbonized shiitake mushrooms. b) XPS and c) FTIR spectra of natural and carbonized mushrooms. d) Physical picture of the system for demonstrating hydrophilicity of the carbonized mushroom. e) Infrared photos of region in dashed box in (d). The photos in order from top to bottom correspond to $t = 0$, 60, 180, and 360 s after the dried carbonized mushroom is in touch with the water. Black dashed lines indicate the contour of the carbonized mushroom.

AM 1.5 G). After the carbonization treatment, the absorption dramatically increased to ≈96% mainly due to the reduced reflection, which is a result of the increased roughness of surface structure after carbonization.

The mushroom maintains its hydrophilicity before and after carbonization because of its components, which include carbohydrates and proteins; the nitrogen functional groups exist even after carbonization. The surface chemical compositions and functional groups of natural and carbonized mushrooms were identified by X-ray photoelectron spectroscopy (XPS) and Fourier transform infrared (FTIR) spectroscopy. Figure 2b displays the XPS spectra of natural and carbonized mushrooms. In addition to C 1s and O 1s, the N 1s signal was also detected. The deconvoluted N 1s spectra of natural and carbonized mushrooms all show a strong peak at ≈399.4 eV (Figure S2, Supporting Information), corresponding to C—N/N—H. Meanwhile, the peaks in FTIR spectra (Figure 2c) for natural and carbonized mushrooms are observed at ≈3346 and 1078 cm^{-1}, 3390 and 1111 cm^{-1}, further confirming the existence of C—N/N—H.

The hydrophilic nature of carbonized mushrooms enables very efficient water supply if the mushroom is floating on the surface of water (Figure 2d). The wetting process of a carbonized mushroom once in touch with water was captured by an infrared camera without illumination (Figure 2e). In this process, the mushroom initially has the same temperature as the water. As the wetting process continues, the evaporation helps to lower the temperature. Only ≈360 s is needed for a mushroom to complete the wetting process without sunlight-assisted transpiration. Furthermore, when a drop of water is placed on the surface of a mushroom, the droplet is absorbed in less than half a second, demonstrating the mushroom's superior hydrophilicity (Video S1, Supporting Information), which is beneficial for efficient solar steam generation.

As mentioned previously, the geometry of mushrooms is also naturally optimized for minimizing all three components of heat loss, which include conduction, convection, and radiation (**Figure 3**a). As a curved surface with a large surface-projected area ratio enables stronger evaporation and consequently smaller temperature increase, convection and radiation losses are expected to be suppressed. The fibrous stipe, while enabling efficient water supply, also confines the water path in a quasi-1D, leading to the minimization of heat conduction loss. An infrared camera was used here to carefully investigate heat behavior in mushroom-based structures under 1 sun intensity. The maximum temperature (T_{max}) and average temperature (T_{av}) are plotted in Figure 3b as a function of illumination time. Typical infrared pictures of the surfaces in natural and carbonized mushrooms are also displayed in Figure 3c. The temperatures of natural and carbonized mushrooms (22 and 21 °C, respectively) were quite low during the initial stage, indicating strong intrinsic evaporation as expected. Once the light was turned on, rapid increases in T_{max} and T_{av} were observed. According to the increasing trend in temperature, ≈840 and ≈630 s are needed for the natural and carbonized mushrooms to obtain quasi-steady states. As expected, after 1 h illumination, T_{max} of the surfaces in natural and carbonized mushrooms reached ≈37.5 and 38 °C, respectively, which were relatively low compared with other absorbers.[16] This result led to a radiation

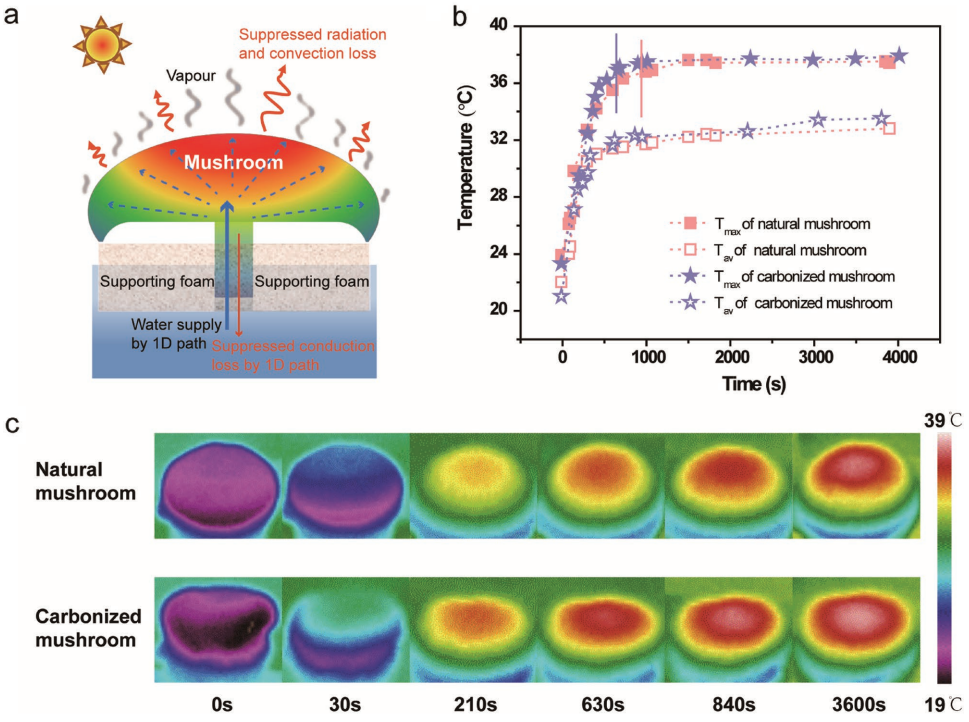

Figure 3. Heat behavior of the mushroom-based structures under 1 sun illumination. a) Schematic of the heat behavior in a mushroom-based structure. b) Maximum and average temperatures of surfaces for natural and carbonized mushrooms as a function of time. The blue and pink lines show the turning points to the quasi-steady state of natural and carbonized mushrooms. c) Infrared photos of the natural and carbonized mushroom surfaces. The photos, in order from left to right, correspond to t = 0, 30, 210, 630, 840, and 3600 s after illumination.

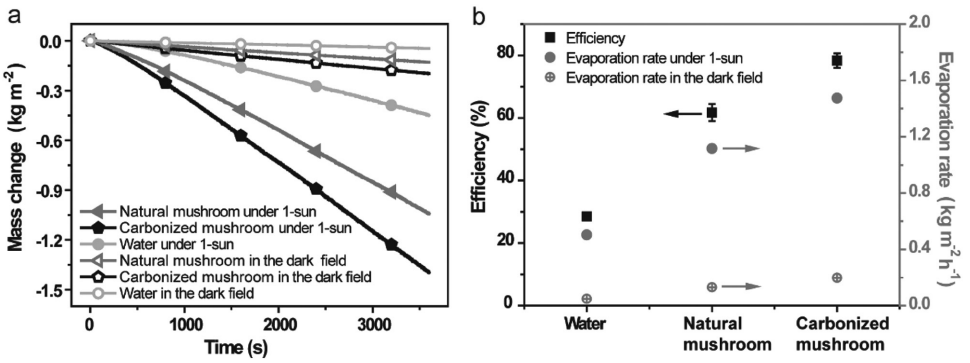

Figure 4. Natural and carbonized mushrooms for solar steam generation. a) Mass change of water over time in the dark field and under 1 sun illumination. b) Solar steam efficiency (black, left hand side axis) and evaporation rate in the dark field and under 1 sun illumination (gray, right-hand side axis) with the natural and carbonized mushrooms.

loss of only ≈4% and ≈6% and a convection loss of only ≈4% and ≈5% (Section S1, Supporting information), respectively, for natural and carbonized mushrooms. The increased absorption of the carbonized mushroom (≈17% increase) resulted in a higher T_{max}. However, the disparity in the T_{max} values of the surfaces of the two mushrooms was quite small. This phenomenon was attributed to the stronger evaporation ability of the carbonized mushrooms that lowered the T_{max} and narrowed the temperature difference between the two. The thermal conductivities of natural and carbonized mushrooms were measured to be ≈0.28 and ≈0.45 W m^{-1} K^{-1}, respectively (Table S2, Supporting Information). The low thermal conductivities together with the quasi-1D conductive path caused a conductive loss for both natural and carbonized mushrooms of less than 1%. The calculation details of heat loss can be found in Section S1 (Supporting Information).

To systematically evaluate the performance of a mushroom-based solar steam device (Figure S3, Supporting Information), the evaporation rates and energy conversion efficiencies were accurately examined by recording the weight change under normal solar illumination (1 kW m^{-2}) in beakers. Typical curves of time-dependent mass change under various conditions are plotted in **Figure 4**a. The evaporation rates were calculated from the slope of the curves. Because of the larger evaporating areas and porous and fibrous microstructures, the intrinsic evaporating abilities of natural and carbonized mushrooms are 0.13 and 0.198 kg m^{-2} h^{-1}, respectively, which were much higher than that of pure water (0.048 kg m^{-2} h^{-1}). After the light had been turned on, the steady-state evaporations of natural and carbonized mushrooms were achieved after ≈800 and ≈600 s illumination, which coincided well with the time for the surfaces of two samples to achieve a steady temperature (Figure 3b). Finally, the evaporation rates were calculated to be 1.116 and 1.475 kg m^{-2} h^{-1}, which were 2.2 and 2.9 times that of pure water (0.503 kg m^{-2} h^{-1}), as shown in Figure 4b.

The energy conversion efficiency is defined as $\eta = \dot{m}h_{lv}/P_{in}$, where $\dot{m}$ is the mass flux of steam, h_{lv} denotes the liquid–vapor phase change enthalpy, and P_{in} is the received power density of solar illumination. For our structures, the efficiencies were calculated to be 62% and 78% for mushrooms before and after carbonization at the power density of 1 kW m^{-2}. Carbonized mushrooms also demonstrated good mechanical properties, and their typical compressive stress was 8 MPa (Figure S4, Supporting Information). Thus, carbonized mushrooms performed stably in solar steam generation over eight cycles (Figure S5, Supporting Information) with 3600 s irradiation each cycle, showing good stability.

In conclusion, we have shown that mushrooms, often hidden from sunlight, enable efficient solar steam generation because their natural structures possess the excellent properties of light absorption, thermal management with minimized heat loss, and efficient water supply and vapor escape. These findings not only revealed the hidden talent of mushrooms as low-cost materials ($2 per kg) for solar steam generation but also provided inspiration for the future development of high-performance solar thermal conversion devices.

Experimental Section

Materials Preparation: Dried shiitake mushrooms used in experiments were purchased from local supermarkets. These mushrooms were first soaked in water for 3 h to soften them and then repeated draining and soaking them in deionized water several times to clean them. The mushrooms were then treated at 500 °C in Ar for 12 h to obtain carbonized mushrooms.

Materials Characterization: The morphologies and nanostructures of natural and carbonized shiitake mushrooms were characterized by scanning electron microscopy (Dual-beam FIB 235, FEI Strata). XPS spectra were obtained using a THERMO FISHERSCIENTIFIC K-Alpha instrument. FTIR spectra were obtained on a Nexus 870 spectrometer. The natural shiitake mushroom was dried by a general freeze-drying method for SEM, XPS, and FTIR tests. The optical transmittance and reflectance spectra of the surfaces of natural and carbonized mushrooms were measured in the range of 200–2500 nm with a Shimadzu UV3600 spectrophotometer attached to an integrating sphere (ISR-3100). Wet pileus was used for this measurement as it was closest to the working condition. The absorption efficiency was then calculated by $A = 1 - R - T$, where R and T are the reflection and transmission efficiency, respectively. FLUKE Ti 100 infrared camera was used to take infrared photographs. Mechanical tests were performed on a Microcomputer Control Electronic Universal Testing Machine made by REGER in China (RGWT-4000-5) (Figure S5, Supporting Information). The thermal diffusivity was measured by Netzsch LFA 467 Nanoflash, and the specific heat capacity was measured by differential scanning calorimetry (DSC, Perkin Elmer DSC8000) (Table S2, Supporting Information).

Experimental Setup for Steam Generation: Mushroom-Based Structure: A natural/carbonized mushroom was placed in a punched polystyrene

foam (thermal conductivity ≈0.04 W m k^{-1}) with the stipe inserted in the hole, and the entire structure was allowed to float on the surface of water with only the bottom side of the stipe in direct contact with bulk water.

The experiments were typically conducted at an ambient *T* of ≈28 °C and a humidity of ≈41%. Natural and carbonized mushrooms were floated on the water in 25 and 10 mL beakers, respectively, since the carbonized mushroom had decreased in size by 30% after carbonization. The steam-generation experiments were performed under a homemade optical system, with a solar simulator (Newport 94043A, AM1.5). Once the light was on, the mass change was immediately tracked by a high-accuracy balance (FA 2004, 0.1 mg in accuracy) and then real-time communicated to a desktop computer (with RS 232 serial ports) for calculating the evaporation rate and efficiency of solar steam generation. The respective evaporation rates in the dark field were subtracted from all the measured evaporation rates under 1 sun to identify the effect of solar illumination on evaporation rates and obtain accurate energy conversion efficiencies. The thermal diffusivity was measured by a Netzsch LFA 467 Nanoflash, and the specific heat capacity was measured by DSC (Perkin Elmer DSC8000).

Supporting Information

Supporting Information is available from the Wiley Online Library or from the author.

Acknowledgements

N.X. and X.H. contributed equally to this work. The authors acknowledge the microfabrication centre of the National Laboratory of Solid State Microstructures (NLSSM) for technical support. This work was jointly supported by the State Key Program for Basic Research of China (No. 2015CB659300), the National Natural Science Foundation of China (Nos. 11321063 and 11574143), the Natural Science Foundation of Jiangsu Province (Nos. BK20150056 and BK20160630), the Project Funded by the Priority Academic Program Development of Jiangsu Higher Education Institutions (PAPD), and the Fundamental Research Funds for the Central Universities.

Conflict of Interest

The authors declare no conflict of interest.

Keywords

absorption, heat loss, hydrophilic, mushrooms, solar steam generation

Received: December 14, 2016
Revised: April 11, 2017
Published online: May 18, 2017

[1] L. Y. Tan, J. Wang, W. Xu, Y. Yuan, W. Cai, S. Zhu, J. Zhu, *Nat. Photonics* **2016**, *10*, 393.
[2] G. Ni, N. Miljkovic, H. Ghasemi, X. Huang, S. V. Boriskina, C. T. Lin, J. Wang, Y. Xu, M. M. Rahman, T. Zhang, G. Chen, *Nano Energy* **2015**, *17*, 290.
[3] H. Jin, G. Lin, L. Bai, A. Zeiny, D. Wen, *Nano Energy* **2016**, *28*, 397.
[4] X. Hu, W. Xu, L. Zhou, Y. Tan, Y. Wang, S. Zhu, J. Zhu, *Adv. Mater.* **2017**, *29*, 1604031.
[5] J. Lou, Y. Liu, Z. Wang, D. Zhao, C. Song, J. Wu, N. Dasgupta, W. Zhang, D. Zhang, P. Tao, W. Shang, T. Deng, *ACS Appl. Mater. Interfaces* **2016**, *8*, 14628.
[6] O. Neumann, C. Feronti, A. D. Neumann, A. Dong, K. Schell, B. Lu, E. Kim, M. Quinn, S. Thompson, N. Grady, P. Nordlander, M. Oden, N. J. Halas, *Proc. Natl. Acad. Sci. USA* **2013**, *110*, 11677.
[7] K. Bae, G. Kang, S. K. Cho, W. Park, K. Kim, W. J. Padilla, *Nat. Commun.* **2015**, *6*, 10103.
[8] O. Neumann, A. S. Urban, J. Day, S. Lal, P. Nordlander, N. J. Halas, *ACS Nano* **2013**, *7*, 42.
[9] D. Zhao, H. Duan, S. Yu, Y. Zhang, J. He, X. Quan, P. Tao, W. Shang, J. Wu, C. Song, T. Deng, *Sci. Rep.* **2015**, *5*, 17276.
[10] M. S. Zielinski, J. W. Choi, T. La Grange, M. Modestino, S. M. Hashemi, Y. Pu, S. Birkhold, J. A. Hubbell, D. Psaltis, *Nano. Lett.* **2016**, *16*, 2159.
[11] J. Huang, C. Liu, Y. Zhu, S. Masala, E. Alarousu, Y. Han, A. Fratalocchi, *Nat. Nanotechnol.* **2016**, *11*, 60.
[12] L. Zhou, Y. L. Tan, D. X. Ji, B. Zhu, P. Zhang, J. Xu, Q. Q. Gan, Z. F. Yu, J. Zhu, *Sci. Adv.* **2016**, *2*, e1501227.
[13] L. Tian, J. Luan, K. K. Liu, Q. Jiang, S. Tadepalli, M. K. Gupta, R. R. Naik, S. Singamaneni, *Nano. Lett.* **2016**, *16*, 609.
[14] G. Ni, G. Li, Svetlana V. Boriskina, H. Li, W. Yang, T. Zhang, G. Chen, *Nat. Energy.* **2016**, *1*, 16126.
[15] X. Li, W. Xu, M. Tang, L. Zhou, B. Zhu, S. Zhu, J. Zhu, *Proc. Natl. Acad. Sci. USA* **2016**, *113*, 13953.
[16] Y. Ito, Y. Tanabe, J. Han, T. Fujita, K. Tanigaki, M. Chen, *Adv. Mater.* **2015**, *27*, 4302.
[17] L. Zhang, B. Tang, J. Wu, R. Li, P. Wang, *Adv. Mater.* **2015**, *27*, 4889.
[18] Q. Jiang, L. Tian, K. K. Liu, S. Tadepalli, R. Raliya, P. Biswas, R. R. Naik, S. Singamaneni, *Adv. Mater.* **2016**, *28*, 9400.
[19] H. Ghasemi, G. Ni, A. M. Marconnet, J. Loomis, S. Yerci, N. Miljkovic, G. Chen, *Nat. Commun.* **2014**, *5*, 4449.
[20] S. M. Sajadi, N. Farokhnia, P. Irajizad, M. Hasnain, H. Ghasemi, *J. Mater. Chem. A* **2016**, *4*, 4700.
[21] Y. Wang, L. Zhang, P. Wang, *ACS Sustainable Chem. Eng.* **2016**, *4*, 1223.
[22] D. J. Royse, L. C. Schisler, D. A. Diehle, *Interdiscipl. Sci. Rev.* **2013**, *10*, 329.
[23] J.A. Buswell, Y.J. Cai, S. T. Chang, J.F. Peberdy, S.Y. Fu, H.S. Yu, *World J. Microbiol. Biotechnol.* **1996**, *12*, 537.
[24] F. Liu, V. E. C. Ooi, S. T. Chang, *Life Sci.* **1997**, *60*, 763.
[25] P. Mattila, K. Suonpää, V. Piironen, *Nutrition* **2000**, *16*, 694.
[26] M.-L. Ng, A.-T. Yap, *J. Altern. Complem. Med.* **2002**, *8*, 581.
[27] N. Jasrotia, I. Sharma, S. Badhani, B. Prashar, *Asian J. Pharmacy Life Sci.* **2012**, *2*, 81.
[28] K. Tokimoto, M. Fukuda, M. Tsuboi, *Mycoscience* **1998**, *39*, 217.
[29] P. G. Miles, S. T. Chang, *Mushroom Biology Concise Basics and Current Developments*, World Scientific, Singapore **1997**.
[30] P. García-Segovia, A. Andrés-Bello, J. Martínez-Monzó, *LWT - Food Sci. Technol.* **2011**, *44*, 480.
[31] K. Aydin, V. E. Ferry, R. M. Briggs, H. A. Atwater, *Nat. Commun.* **2011**, *2*, 517.
[32] E. Moulin, J. Sukmanowski, P. Luo, R. Carius, F. X. Royer, H. Stiebig, *J. Non-Cryst. Solids* **2008**, *354*, 2488.
[33] E. Garnett, P. Yang, *Nano Lett.* **2010**, *10*, 1082.
[34] S. K. Kim, H.-S. Ee, W. Choi, S.-H. Kwon, J.-H. Kang, Y.-H. Kim, H. Kwon, H.-G. Park, *Appl. Phys. Lett.* **2011**, *98*, 011109.
[35] K. G. Ong, O. K. Varghese, G. K. Mor, K. Shankar, C. A. Grimes, *Sol. Energy. Mater. Sol. Cells* **2007**, *91*, 250.

